Author Manuscript

Author Manuscript

Author Manuscript

Author Manuscript

HHS Public Access

Author manuscript

Neurobiol Aging. Author manuscript; available in PMC 2024 March 01.

Published in final edited form as:

Neurobiol Aging. 2023 March ; 123: 75–82. doi:10.1016/j.neurobiolaging.2022.12.004.

Signatures for Viral Infection and Inflammation in the Proximal Olfactory System in Familial Alzheimer's Disease

Andrew N. Bubak[1,‡], **Laetitia Merle**[2,3,‡], **Christy S. Niemeyer**[1], **B. Dnate' Baxter**[2,3], **Arianna Gentile Polese**[2,3], **Vijay Ramakrishnan**[4], **Johana Gomez**[5], **Lucia Madrigal**[5], **Andres Villegas-Lanau**[5], **Francisco Lopera**[5], **Wendy Macklin**[1,2], **Seth Frietze**[6], **Maria A. Nagel**[1,7,#], **Diego Restrepo**[1,2,#,*]

[1]Department of Neurology, University of Colorado Anschutz Medical Campus, Aurora, CO 80045, USA

[2]Neuroscience Graduate Program, University of Colorado Anschutz Medical Campus, Aurora, CO 80045, USA

[3]Department of Cell and Developmental Biology, University of Colorado Anschutz Medical Campus, Aurora, CO 80045, USA

[4]Department of Otolaryngology-Head and Neck Surgery, Indiana University School of Medicine, Indianapolis, IN 46202, USA

[5]Neuroscience Research Group, University of Antioquia, Medellín, Colombia

[6]Department of Medical Laboratory Sciences, University of Vermont, Burlington, VT

[7]Department of Opthalmology, University of Colorado Anschutz Medical Campus, Aurora, CO 80045, USA

Abstract

[*]Corresponding author: Diego Restrepo, diego.restrepo@cuanschutz.edu.
[‡]Co-first authors
[#]Senior authors

Disclosure
The authors report no disclosures.

Author statemen
Bubak: Conceptualization, Methodology, Formal Analysis, Investigation, Writing; **Merle:** Conceptualization, Methodology, Formal Analysis, Investigation, Writing; **Niemeyer:** Conceptualization, Investigation; **Baxter:** Methodology, Investigation; **Gentile Polese:** Methodology, Investigation; **Ramakrishnan:** Conceptualization; Gomez: Methodology, Investigation; **Madrigal**: Methodology, Investigation; **Villegas-Lanau:** Conceptualization, Methodology, Investigation, Writing; **Lopera:** Conceptualization, Writing; **Macklin:** Conceptualization, Formal Analysis; **Frietze**: Formal Analysis; **Nagel**: Conceptualization, Methodology, Writing, Funding Acquisition; **Restrepo**: Conceptualization, Methodology, Writing, Funding Acquisition

Verification
The work described has not been published previously and it is not under consideration for publication elsewhere, its publication is approved by all authors and by the responsible authorities where the work was carried out, and that, if accepted, it will not be published elsewhere in the same form, in English or in any other language, including electronically without the written consent of the copyrightholder.
The manuscript has been posted in BioRxiv doi: https://doi.org/10.1101/2022.07.19.500641

Publisher's Disclaimer: This is a PDF file of an unedited manuscript that has been accepted for publication. As a service to our customers we are providing this early version of the manuscript. The manuscript will undergo copyediting, typesetting, and review of the resulting proof before it is published in its final form. Please note that during the production process errors may be discovered which could affect the content, and all legal disclaimers that apply to the journal pertain.

Author Manuscript Author Manuscript Author Manuscript Author Manuscript

Alzheimer's disease (AD) is characterized by deficits in olfaction and olfactory pathology preceding diagnosis of dementia. Here we analyzed differential gene and protein expression in the olfactory bulb (OB) and tract (OT) of familial AD (FAD) individuals carrying the autosomal dominant presenilin 1 E280A mutation. Compared to control, FAD OT had increased immunostaining for β-amyloid (Aβ) and CD68 in high and low myelinated regions, as well as increased immunostaining for Iba1 in the high myelinated region. In FAD samples, RNA sequencing showed: (1) viral infection in the OB; (2) inflammation in the OT that carries information via entorhinal cortex from the OB to hippocampus, a brain region essential for learning and memory; and (3) decreased oligodendrocyte deconvolved transcripts. Interestingly, spatial proteomic analysis confirmed altered myelination in the OT of FAD individuals, implying dysfunction of communication between the OB and hippocampus. These findings raise the possibility that viral infection and associated inflammation and dysregulation of myelination of the olfactory system may disrupt hippocampal function, contributing to acceleration of FAD progression.

1. Introduction

A critical barrier in treating Alzheimer's disease (AD) is the years- to decades-long lag from disease onset to the diagnosis of dementia, when reversal of brain pathology and recovery of neurons may, at best, slow cognitive decline. Thus, it is essential to identify contributory pathological processes in early disease to prevent progression to dementia, disability, and death. An early process in AD, prior to clinical dementia, is a deficit in the sense of smell[1–3] accompanied by amyloid-beta (Aβ) deposition in the olfactory bulb (OB)[4, 5]. The OB receives olfactory input from olfactory sensory neurons in the olfactory epithelium (OE)[3, 6] then transmits olfactory information via the olfactory tract (OT) to the entorhinal cortex and hippocampus, brain regions essential for learning and memory that are affected in AD. Dissecting mechanisms involved in olfactory dysfunction can identify potential diagnostic and therapeutic targets in AD. However, little is known about changes in the cellular processes of the olfactory system, including the OB and OT.

Because sporadic AD is quite heterogenous due to variable contributions of host and environmental factors, we focused our initial studies on olfactory tissues from a well-characterized familial AD (FAD) cohort from Colombia. These FAD individuals have the presenilin 1 E280A mutation and develop mild cognitive impairment (MCI) and dementia at the respective median ages of 44 (95% CI, 43–45) and 49 (95% CI, 49–50) years old[7]. Formalin-fixed paraffin embedded (FFPE) slides containing olfactory tissue collected from this FAD cohort post-mortem, as well as control tissue, were examined for tissue morphology and composition. Adjacent slides were analyzed by targeted RNA sequencing of the OB and OT (TempO-Seq, BioSpyder Technologies, Inc., Carlsbad, CA)[8] and by spatial proteomics (nanoString Technologies, Seattle, WA)[9]; bioinformatics analyses were used to identify significantly enriched gene expression pathways.

Author Manuscript Author Manuscript Author Manuscript Author Manuscript

2. Methods

2.1 Standard Protocol Approvals, Registrations, Patient Consents

Tissue from individuals in Colombia with the presenilin 1 PSEN1 E280A mutation [10] and age-matched controls were collected for this study. Approval for post-mortem studies was granted by the institutional review board committee at the University of Antioquia (Comité de Bioetica de la Sede de Investigación Universitaria, Universidad de Antioquia, Colombia) on June 26th, 2019 (approval number 19010–858). Participants provided written informed consent before participating, agreeing to donate tissue for research at time of death. A total of 6 members from Colombian families with the *PSEN1* E280A mutation and 6 age-matched controls were available for analysis in the study. Demographic data and associated studies completed herein are detailed in Table 1. The average age (range, years [y]) of the control and FAD groups was 69 y (56–84 y) and 62 y (53–86 y), respectively. The control group contained 5 males and 1 female; the FAD group contained 2 males and 4 females. None of the individuals in either control of FAD groups died of viral infection that may affect interpretation of results.

The E280A carriers have a previously documented median expected age at onset of MCI at 44 years of age (95% confidence interval [CI] = 43–45 years) and dementia due to AD at 49 years of age (95% CI = 49–50 years) [7]. Eligible individuals were screened for neurological and psychiatric disorders prior to death, and they did not die of viral pneumonia. At time of death, all 6 FAD individuals had a clinical diagnosis of dementia. Clinical data were stored in a secure database at the Neuroscience Group of Antioquia in Medellín, Colombia.

2.2 Sample Collection

Brain samples were collected post-mortem; tissue containing the OB and OT were fixed in formalin then paraffin-embedded. OB/OT tissue blocks were cut sagittally at 7 μm thickness and placed on slides for hematoxylin and eosin staining (H&E; data not shown) and immunohistochemical (IHC) staining.

2.3 Multispectral Immunohistochemistry of the Olfactory Bulb and Olfactory Tract

Through our collaboration with the Human Immune Monitoring Shared Resource (HIMSR) at the University of Colorado School of Medicine, we performed multispectral imaging using the Akoya Vectra Polaris instrument. This instrumentation allows for phenotyping, quantification, and spatial relationship analysis of tissue infiltrate in formalin-fixed paraffin-imbedded biopsy sections[11].

FFPE tissue sections containing OB and OT were stained consecutively with specific primary antibodies according to standard protocols provided by Akoya and performed routinely by the HIMSR. Briefly, the slides were deparaffinized, heat treated in antigen retrieval buffer, blocked, and incubated with primary antibodies against Aβ, Iba1, GFAP, Cleaved Caspase 3, p-Tau, DCX, CD68, and PLP (Supplemental Table 1), followed by horseradish peroxidase (HRP)-conjugated secondary antibody polymer, and HRP-reactive OPAL fluorescent reagents that use TSA chemistry to deposit dyes on the tissue immediately surrounding each HRP molecule. To prevent further deposition of fluorescent

Author Manuscript Author Manuscript Author Manuscript Author Manuscript

dyes in subsequent staining steps, the slides were stripped in between each stain with heat treatment in antigen retrieval buffer. Slides were finally counterstained with DAPI. Whole slide scans were collected using the 10x objective and multispectral images were collected using the 20x objective with a 0.5 micron resolution. The 9-color images were analyzed with inForm software V2.5 to unmix adjacent fluorochromes, subtract autofluorescence, segment the tissue, compare the frequency and location of cells, segment cellular membrane, cytoplasm, and nuclear regions, score each cellular compartment, and phenotype infiltrating immune cells according to morphology and cell marker expression.

We used custom scripts in Fiji to quantify Aβ, Iba1, CD68 and PLP on the 20x objective images; GFAP, Cleaved Caspase 3, p-Tau, and DCX antibodies did not yield reliable staining and were not further analyzed. ROIs for high and low myelinated areas were manually determined using PLP stain by two researchers. To quantify Aβ, Iba1 and CD68-positive areas, we defined the positive area as one that exceeds n SDs of the mean image intensity, with $n = 2$ for Aβ and Iba1 and $n = 4$ for CD68. The positive surface was expressed as a percentage of the ROI surface per individual. Masks for each stain were created from the thresholded images, and mask combinations were used to determine the double and triple-positive areas.

2.4 FFPE TempO-Seq

For whole human transcriptome analysis, FFPE slides containing OB or OT were assayed using TempO-Seq–targeted RNA sequencing plates, reagents, protocols, and software (BioSpyder Technologies)[8]. TempO-Seq exclusively detects human transcripts; viral transcripts were not assayed. H&E stained tissue sections were used to distinguish the OB from OT. Of the 6 controls, only 4 had adequate samples for this analysis whereas all 6 FAD samples contained OB and OT for this analysis. The OB and OT from adjacent, non-stained slides were separately scraped (~5–10 mm^2) and placed into PCR tubes containing 1X lysis buffer. Using a thermocycler, samples containing OB or OT were lysed. Coded adjacent primer pairs for each specific human transcript were annealed to sample RNA; primer pairs for each transcript were ligated and then amplified per manufacturer's instructions and as previously described [12]. If a transcript is present, the adjacent 25-nucleotide primer pairs anneal to their specific target, ligate together, and produce a 50-nucleotide transcript-specific, coded amplicon.

Amplified PCR products were pooled into a single library, concentrated using a PCR cleanup kit (Macherey-Nagel, Düren, Germany), and run on the Illumina NextSeq 500 sequencing platform (Illumina Inc., San Diego, CA). Mapped reads were generated by TempO-SeqR for the alignment of demultiplexed FASTQ files from the sequencer to the ligated detector oligomer gene sequences using Bowtie, allowing for up to 2 mismatches in the 50-nucleotide target sequence[8]. Counts were assessed using SARTools[13]. Within this R package, edgeR is used for normalization and quality control of count data[14]. Differential expression between groups was assessed by the TempO-SeqR software, which used the DESeq2 method for differential analysis of count data[15]. A significantly differentially expressed gene is defined as having an adjusted p value < 0.05 with no fold-change threshold.

Author Manuscript Author Manuscript Author Manuscript Author Manuscript

Pathway enrichment analysis was performed using gene sets and pathways defined in the Ingenuity Pathway Analysis software (Qiagen, Germantown, MD) and the ClusterProfiler package[16, 17] in R with default parameters. ClusterProfiler supports enrichment analysis of Gene Ontology and Kyoto Encyclopedia of Genes and Genomes databases with Gene Set Enrichment Analysis (GSEA) to identify biological themes of a collection of genes. These functional enrichment analyses use computational approaches to identify groups of experimentally observed human genes that are overrepresented or depleted in a curated disease or biological function-specific gene set. Additional figures were created using Prism 9 (GraphPad Software, San Diego, CA).

2.5 nanoString Proteomics

We used nanoString proteomics for 88 proteins (Supplemental Table 2 with four fluorescent markers to discriminate tissue regions (Supplemental Table 3) using methods detailed by Merritt and co-workers[9]. Briefly, all assays were performed on 7-μm FFPE sections mounted onto charged slides; these slides were adjacent to those used for TempO-Seq analysis. Deparaffinization and rehydration of tissue was performed by incubating slides in three washes of CitriSolv (Decon Labs, 1601) for 5 minutes each, two washes of 100% ethanol for 10 minutes each, two washes of 95% ethanol for 10 minutes each and two washes of distilled water for 5 minutes each. For antigen retrieval, slides were then placed in a plastic Coplin jar containing 1× Citrate Buffer pH 6.0 (Sigma, C9999) and covered with a lid. The Coplin jar was placed into a pressure cooker (BioSB, BSB7008) that was run at high pressure and temperature for 15 minutes. The Coplin jar was removed from the pressure cooker and cooled at room temperature for 25 minutes. Slides were washed with five changes of 1× TBS-T (Cell Signaling Technology, 9997) for 2 minutes each. Excess TBS-T was removed from the slide, and a hydrophobic barrier was drawn around each tissue section with a hydrophobic pen (Vector Laboratories, H-4000). Slides were then incubated with blocking buffer (1× TBS-T, 5% goat serum (Sigma-Aldrich, G9023–5ML), 0.1 mg ml–1 salmon sperm DNA (Sigma-Aldrich, D7656) and 10 mg ml–1 dextran sulfate (Sigma-Aldrich, 67578–5G) for 1 hour. Slides were washed with three changes of 1× TBS-T for 2 minutes each. Primary antibodies (Supplemental Tables 2 and 3) were diluted in Buffer W (GeoMx Protein Slide Prep Kit Item 121300312). Tissue sections were then covered with diluted primary antibody solution (see above for morphology marker information). Slides were incubated at 4°C in a humidity chamber overnight. Primary antibody was aspirated from slides, and slides were washed with three changes of 1× TBS-T for 10 minutes each. Antibodies were postfixed with 4% paraformaldehyde for 30 minutes at room temperature and then wasted twice in TBS-T. DNA was counterstained with 500 nM SYTO13 (Thermo Fisher, S7575) in 1× TBS-T or TBS for 15 minutes. Excess DNA counterstain was removed with five changes of TBS-T, and slides were the processed on the GeoMx instrument as described in Merritt et al.[9].

2.6 Statistical Analysis

Matlab or Excel were used to perform t tests or ANOVAs, followed by post-hoc Fisher's least significant difference procedure.

Author Manuscript Author Manuscript Author Manuscript Author Manuscript

2.7 Data Availability

All data used in the analyses of this study are available within the manuscript and its supplemental information files. Raw gene counts generated from the TempO-Seq analysis are deposited in the NCBI Gene Expression Omnibus database. Requests for further data sharing including individual patient sample information will be reviewed by the corresponding author and appropriate regulatory bodies with respect to maintaining de-identified status.

3. Results

3.1 Immunohistochemical analysis shows Aβ and microglia/macrophages in FAD olfactory tissue.

Prior to transcriptome analysis, we analyzed the tissue for morphology and composition. Figure 1 A–C shows immunohistochemical analysis of the human OT from FAD subjects and age-matched controls (Table 1). Staining for the myelin marker proteolipid protein (PLP)[18] showed that the OT included high and low myelination areas (Figure 1A). We did not find a difference between FAD and controls in the area occupied by the high/low myelinated regions in the OT (Figure 1A). As expected, we found increased immunostaining for Aβ in the OT of FAD subjects compared to controls (Figure 1B). In addition, as expected for neuroinflammation in AD, and consistent with prior studies in spontaneous AD[19], we found increased immunostaining for the microglia/macrophage markers Iba1 and CD68 in FAD OT compared to control (Figure 1C). Finally, we found increased association between CD68 and Iba1 and between Aβ and microglia whose association has been proposed to constitute a barrier with profound impact on Aβ plaque composition and toxicity[20] (Figure 1D–E).

3.2 Targeted RNA sequencing shows enrichment of pathways involved in virus infection in OB and of inflammation in OT.

We then performed TempO-seq targeted RNA sequencing analysis of the OB and OT from 6 FAD individuals who did not die of virus infection and 4 age-matched controls (Table 1). Compared to controls, we found 2,775 differentially expressed genes (DEGs) in FAD OB and 1,319 significantly DEGs in FAD OT. Volcano plots in Figures 2Ai (OB) and 2Aii (OT) show that the majority of DEGs displayed increased expression in FADs (also see Supplemental Tables 4 and 5). Human gene-set enrichment analyses in the FAD OB showed multiple upregulated transcriptional pathways associated with viral infection, including “Viral infection”, “Infection of cells”, and “Replication of virus” (Figure 2Aiii), whereas the OT of FAD individuals represented an upregulation of immune response signatures that included “IL-6 signaling”, “IL-8 signaling”, “Natural killer cell signaling”, “Jak/Stat signaling”, “Neuroinflammation signaling”, and “Production of nitric oxide and reactive oxygen species in macrophages,” as well as the expected “Amyloid processing” pathway (Figure 2Aiv). Observed genes in each pathway are shown in Supplemental Table 6. When we deconvolved the DEGs to estimate glial surrogate proportions, we found that microglia were higher in FAD OT samples (Figure 2C), consistent with the immunohistochemistry results for Iba1 and CD68 (Figure 1C). Interestingly, in the deconvolution, we found a decreased surrogate proportion for oligodendrocytes in OT in FAD (Figure 2C). No

Author Manuscript Author Manuscript Author Manuscript Author Manuscript

differences in glial surrogate proportions were observed in FAD OB samples compared to controls (not shown).

3.3 Spatial proteomics assay shows changes consistent with a demyelination response in the OT of FAD samples.

We performed complementary nanoString spatial proteomics analysis[9] for 88 proteins including markers for AD and immune responses (Supplemental Table 2) in tissue regions discriminated based on fluorescent markers for myelin basic protein, Aβ, Iba1 and nuclear staining (see Methods and Supplemental Table 3). The four tissue regions were high myelination and low myelination OT, and glomerular layer/external plexiform layer and granule cell layer in the OB (Figure 3A, Supplemental Figure 1). nanoString proteomics showed spatial protein specificity involved in immune and AD responses in the OT and to a lesser extent in the OB (Figure 3B). Interestingly, both the immune and AD marker responses differ between regions. For example, the increase in AD markers in FAD was most marked in the low myelinated OT, and there were increases in immune markers in both low and high myelinated OT, but they were heterogeneous between these two brain regions and much lower in the OB indicating that the immune response differs between brain areas in the proximal olfactory system (Figure 3B). Strikingly, principal component analysis (PCA) of the spatial proteomics results shows orthogonal localization of FAD versus control proteomics regardless of the tissue region (Figure 3C). Furthermore, there were marked differences in protein expression between brain regions within the experimental groups (FAD and control, Figure 3D and Supplemental Figure 2). Interestingly, within the FAD cohort a large group of proteins involved in response to demyelination were expressed at high levels in high myelination OT compared to all other regions (group A in Figure 3Dii) and a group of AD markers was expressed at high levels in the low myelination OT (group B in Figure 3Dii) (eNote 1). Taken together with the deconvolution of the transcriptome in the OT showing decreased oligodendrocyte in FAD (Figure 3B) these data indicate that there is dysregulation of myelination in FAD.

4. Discussion

Using novel regional/spatial transcriptomic and proteomic assays, we were able to determine gene expression changes in FFPE olfactory tissues from control and FAD samples. Our findings reveal a transcriptomic signature for viral infection in the OB coupled with inflammation and dysregulation of myelination in the OT in FAD samples compared to control samples; results were confirmed by proteomic analysis. While our studies only identified human transcripts/proteins and were not designed to identify specific viruses, the most likely viruses contributing to olfactory system infection and potential CNS dysfunction are the 2 neurotropic alphaherpesviruses, herpes simplex virus type-1 (HSV-1) and varicella zoster virus (VZV). HSV-1 and VZV are strong candidates for being initiators or accelerators of AD because they increase dementia risk and elicit the same pathological characteristics of AD, including amyloid accumulation, neuroinflammation, neurodegeneration, and cognitive impairment[21–23]. Furthermore, this family of alphaherpesviruses is latent in trigeminal ganglia which innervates the OE/OB[24] (Figure 4A, B), providing a direct internal route of virus entry during reactivation.

Author Manuscript Author Manuscript Author Manuscript Author Manuscript

Our studies find that even in patients predisposed to AD due to a genetic mutation of PS1 there is evidence of viral infection in the OB suggesting that viral infection and inflammatory response in the OT are part of the etiology of the disease. In addition, we find a transcriptome signature for inflammation, and proteome differences in response to demyelination in the OT of FAD subjects compared to controls. The OT provides communication between the OB and the hippocampus raising the question whether the viral infection, inflammation and impaired response to demyelination decrease the communication through gamma oscillations between the OB and the hippocampus (Figure 4C,D), and whether this loss in communication alters cognition. Taken together with a parallel body of literature indicating that early AD is characterized by olfactory impairment[1–3], amyloid deposition in the olfactory epithelium (OE), and olfactory sensory neuron (OSN) dysfunction[4, 5], our study raises the possibility that viral infection of the OB/OT accelerates AD. Because sniff-induced beta and theta-coupled gamma oscillations generated in the OB are directionally coupled to the hippocampus[25–28], olfactory impairment would result in decreased hippocampal gamma oscillations that have been postulated to lead to neurodegeneration and cognitive decline[29–31]. These studies suggest that viral disruption of olfactory pathways can accelerate AD cognitive decline.

A limitation in our study was that we only probed for human transcripts and proteins and although strong host viral signaling pathways were identified, whether this is a broad anti-viral response or representative of a specific pathogen is unknown. Follow-up studies investigating specific viral species, such as alphaherpesviruses, in the olfactory system of AD samples are warranted. However, this may be challenging in late-stage tissues harvested at autopsies because viral infection will have likely been cleared yet chronic inflammatory processes representative of an anti-viral response may persist. Amongst all cadidate pathogens, the most likely are HSV-1 and VZV because they are latent in sensory neurons of the TG and have a direct route of entry to the OE and OB by tranxsaxonal spread following recurrent reactivations through an individuals' lifespan. Because viral encephalitis is not observed at high levels in patients with AD, it is likely these pathogens are suppressed early on in the OB and OT. Overall, the transcriptional profile we have observed in this study may be representative of a routinely barraged olfactory system by pathogens and the resulting pathological ramifications such as amyloid deposition, microglia activation, and potentially myelination alterations.

Supplementary Material

Refer to Web version on PubMed Central for supplementary material.

Acknowledgements

The authors thank the subjects and their families for donating brain tissue and Cathy Allen for manuscript preparation. TempO-Seq and nanoString graphics were created with BioRender.com.

Funding

This work was supported by Administrative Supplement grants NIDCD DC014253 and DC000566 from the NIH/NIA to D. Restrepo and a subcontract of MH128867 (Shepherd and Presse) to D. Restrepo.

Author Manuscript Author Manuscript Author Manuscript Author Manuscript

References

1. Wheeler PL, Murphy C. Olfactory Measures as Predictors of Conversion to Mild Cognitive Impairment and Alzheimer's Disease. Brain Sciences 2021;11.
2. Murphy C.Olfactory and other sensory impairments in Alzheimer disease. Nat Rev Neurol 2019;15:11–24. [PubMed: 30532084]
3. Dibattista M, Pifferi S, Menini A, Reisert J. Alzheimer's Disease: What Can We Learn From the Peripheral Olfactory System? Frontiers in Neuroscience 2020;14:440. [PubMed: 32508565]
4. Tremblay C, Serrano GE, Intorcia AJ, et al. Olfactory Bulb Amyloid-β Correlates With Brain Thal Amyloid Phase and Severity of Cognitive Impairment. Journal of Neuropathology & Experimental Neurology 2022;81:643–649. [PubMed: 35751438]
5. Wesson DW, Levy E, Nixon RA, Wilson DA. Olfactory Dysfunction Correlates with Amyloid-β Burden in an Alzheimer's Disease Mouse Model. The Journal of Neuroscience 2010;30:505. [PubMed: 20071513]
6. Attems J, Walker L, Jellinger KA. Olfactory bulb involvement in neurodegenerative diseases. Acta Neuropathologica 2014;127:459–475. [PubMed: 24554308]
7. Acosta-Baena N, Sepulveda-Falla D, Lopera-Gómez CM, et al. Pre-dementia clinical stages in presenilin 1 E280A familial early-onset Alzheimer's disease: a retrospective cohort study. The Lancet Neurology 2011;10:213–220. [PubMed: 21296022]
8. Trejo CL, Babic M, Imler E, et al. Extraction-free whole transcriptome gene expression analysis of FFPE sections and histology-directed subareas of tissue. PLoS One 2019;14:e0212031.
9. Merritt CR, Ong GT, Church SE, et al. Multiplex digital spatial profiling of proteins and RNA in fixed tissue. Nature Biotechnology 2020;38:586–599.
10. Quiroz YT, Sperling RA, Norton DJ, et al. Association Between Amyloid and Tau Accumulation in Young Adults With Autosomal Dominant Alzheimer Disease. JAMA Neurology 2018;75:548–556. [PubMed: 29435558]
11. Parra ER, Uraoka N, Jiang M, et al. Validation of multiplex immunofluorescence panels using multispectral microscopy for immune-profiling of formalin-fixed and paraffin-embedded human tumor tissues. Scientific Reports 2017;7:13380. [PubMed: 29042640]
12. Bubak AN, Como CN, Hassell JE, et al. Targeted RNA Sequencing of VZV-Infected Brain Vascular Adventitial Fibroblasts Indicates That Amyloid May Be Involved in VZV Vasculopathy. Neurology - Neuroimmunology Neuroinflammation 2022;9:e1103. [PubMed: 34759019]
13. Varet H, Brillet-Gueguen L, Coppee JY, Dillies MA. SARTools: A DESeq2- and EdgeR-Based R Pipeline for Comprehensive Differential Analysis of RNA-Seq Data. PLoS One 2016;11:e0157022.
14. Robinson MD, McCarthy DJ, Smyth GK. edgeR: a Bioconductor package for differential expression analysis of digital gene expression data. Bioinformatics 2010;26:139–140. [PubMed: 19910308]
15. Love MI, Huber W, Anders S. Moderated estimation of fold change and dispersion for RNA-seq data with DESeq2. Genome Biol 2014;15:550. [PubMed: 25516281]
16. Yu G, Wang L-G, Han Y, He Q-Y. clusterProfiler: an R Package for Comparing Biological Themes Among Gene Clusters. OMICS: A Journal of Integrative Biology 2012;16:284–287. [PubMed: 22455463]
17. Yu G, Wang L-G, Yan G-R, He Q-Y. DOSE: an R/Bioconductor package for disease ontology semantic and enrichment analysis. Bioinformatics 2015;31:608–609. [PubMed: 25677125]
18. Yamamura T, Konola JT, Wekerle H, Lees MB. Monoclonal Antibodies Against Myelin Proteolipid Protein: Identification and Characterization of Two Major Determinants. Journal of Neurochemistry 1991;57:1671–1680. [PubMed: 1717653]
19. Kohl Z, Schlachetzki JCM, Feldewerth J, et al. Distinct Pattern of Microgliosis in the Olfactory Bulb of Neurodegenerative Proteinopathies. Neural Plasticity 2017;2017:3851262.
20. Condello C, Yuan P, Schain A, Grutzendler J. Microglia constitute a barrier that prevents neurotoxic protofibrillar Aβ42 hotspots around plaques. Nature Communications 2015;6:6176.

Author Manuscript Author Manuscript Author Manuscript Author Manuscript

21. Eimer WA, Vijaya Kumar DK, Navalpur Shanmugam NK, et al. Alzheimer's Disease-Associated beta-Amyloid Is Rapidly Seeded by Herpesviridae to Protect against Brain Infection. Neuron 2018;99:56–63 e53. [PubMed: 30001512]
22. Readhead B, Haure-Mirande JV, Funk CC, et al. Multiscale Analysis of Independent Alzheimer's Cohorts Finds Disruption of Molecular, Genetic, and Clinical Networks by Human Herpesvirus. Neuron 2018;99:64–82 e67. [PubMed: 29937276]
23. Itzhaki RF, Lathe R. Herpes Viruses and Senile Dementia: First Population Evidence for a Causal Link. J Alzheimers Dis 2018;64:363–366. [PubMed: 29889070]
24. Schaefer ML, Bottger B, Silver WL, Finger TE. Trigeminal collaterals in the nasal epithelium and olfactory bulb: a potential route for direct modulation of olfactory information by trigeminal stimuli. J Comp Neurol 2002;444:221–226. [PubMed: 11840476]
25. Martin C, Beshel J, Kay LM. An olfacto-hippocampal network is dynamically involved in odor-discrimination learning. JNeurophysiol 2007;98:2196–2205. [PubMed: 17699692]
26. Gourevitch B, Kay LM, Martin C. Directional coupling from the olfactory bulb to the hippocampus during a go/no-go odor discrimination task. J Neurophysiol 2010;103:2633-2641.
27. Nguyen Chi V, Muller C, Wolfenstetter T, et al. Hippocampal Respiration-Driven Rhythm Distinct from Theta Oscillations in Awake Mice. J Neurosci 2016;36:162–177. [PubMed: 26740658]
28. Pena RR, Medeiros DdC LdO, et al. Home-cage odors spatial cues elicit theta phase/gamma amplitude coupling between olfactory bulb and dorsal hippocampus. Neuroscience 2017;363:97–106. [PubMed: 28890054]
29. Iaccarino HF, Singer AC, Martorell AJ, et al. Gamma frequency entrainment attenuates amyloid load and modifies microglia. Nature 2016;540:230–235. [PubMed: 27929004]
30. Gillespie Anna K, Jones Emily A, Lin Y-H, et al. Apolipoprotein E4 Causes Age-Dependent Disruption of Slow Gamma Oscillations during Hippocampal Sharp-Wave Ripples. Neuron 2016;90:740–751. [PubMed: 27161522]
31. Salimi M, Tabasi F, Abdolsamadi M, et al. Disrupted connectivity in the olfactory bulb-entorhinal cortex-dorsal hippocampus circuit is associated with recognition memory deficit in Alzheimer's disease model. Scientific Reports 2022;12:4394. [PubMed: 35292712]

Author Manuscript Author Manuscript Author Manuscript Author Manuscript

Highlights

- Olfactory impairment is an early symptom of Alzheimer's disease (AD)
- We perform transcriptome analysis of the olfactory bulb (OB) in familial AD (FAD)
- Results suggest viral infection in the OB and inflammation in the OT of FAD patients
- nanoString proteomics found dysregulation of myelination in FAD
- Results imply an impairment in communication between the OB and hippocampus in FAD
- Virus disruption of olfactory pathways could accelerate AD cognitive decline

Author Manuscript Author Manuscript Author Manuscript Author Manuscript

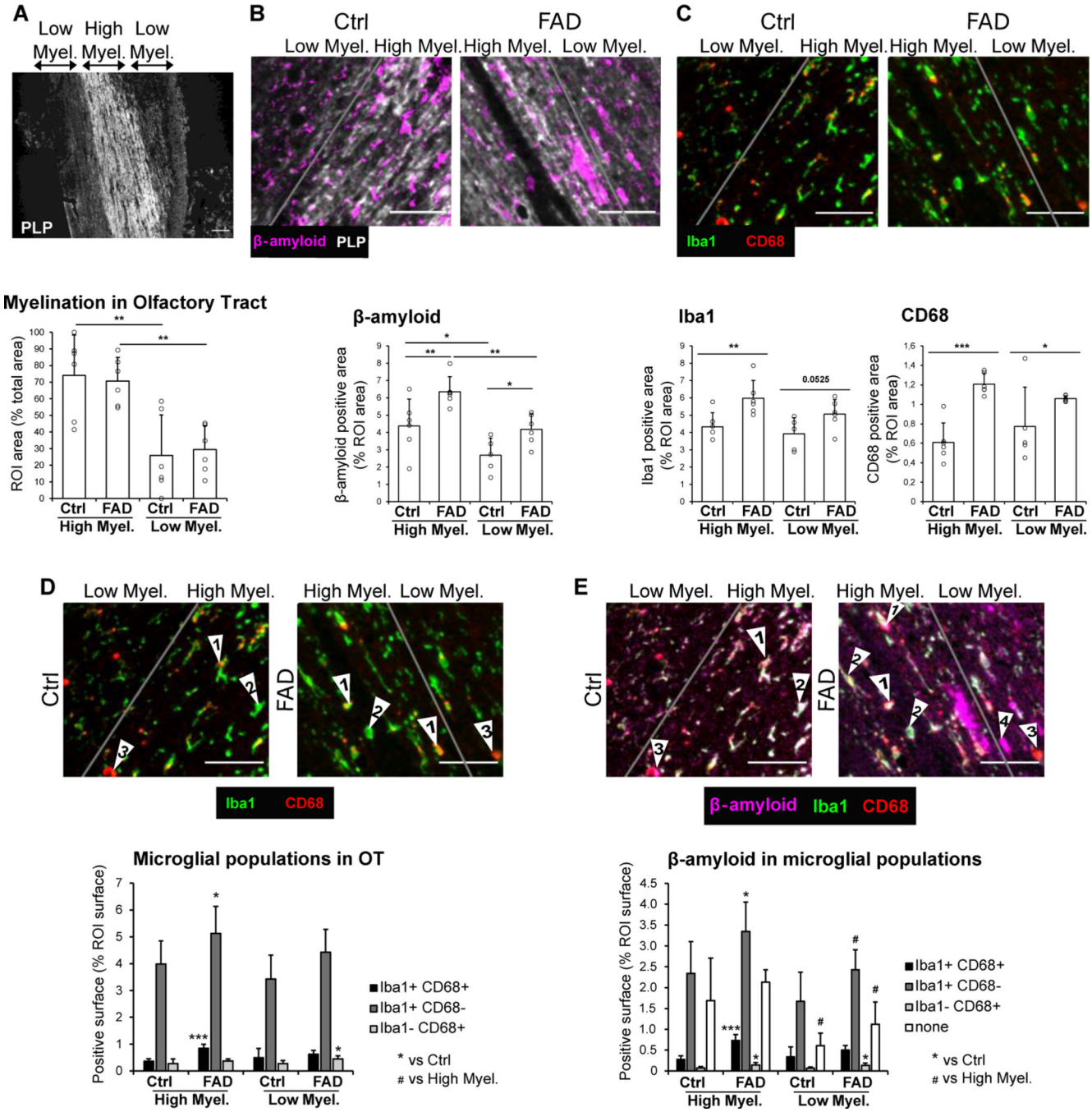

Figure 1.

Immunohistochemistry of the Human OT and TempO-Seq Transcriptome Analysis of the OB and OT

(A-C) IHC of the human OT for 6 control and 6 FAD subjects. (A) PLP stain was used to delimitate the high and low myelinated regions in OT. The bar graph represents the mean surface of high and low myelinated regions per individual, expressed as a percentage of the total area analyzed. An ANOVA yields no significant difference for the genotype F=0.1, 1 d.f., p>0.05 and a significant difference between high and low myelination areas

Author Manuscript Author Manuscript Author Manuscript Author Manuscript

F=26.84, 1 d.f., $p<0.001$. (B) Representative images and quantification of Aβ in the OT from 6 Ctrl and 6 FAD patients. Aβ positive surface is increased in FAD patients compared to control, in both the high and low myelinated OT. Within the FAD group, the accumulation of Aβ is higher in the high myelinated than the low myelinated OT. ANOVA yields a significant difference for the genotype F=13.94, 1 d.f., $p<0.01$ and a significant difference between high and low myelination areas F=17.22, 1 d.f., $p<0.001$. (C) Quantification of microglia/macrophage markers Iba1 and CD68, showing increased neuroinflammation in the high myelinated OT. ANOVA for Iba1 and CD68 yields a significant difference for genotype (Iba1, F=13.54, 1 d.f., $p<0.01$, CD68, F=23.24, 1 d.f., $p<0.001$). (D and E) Quantification of overlap in expression of Aβ, Iba1 and CD68. (D) Quantification of the 3 different microglial populations: Iba1+CD68+ (arrows “1”), Iba1+CD68- (arrows “2”), Iba1-CD68+ (arrows “3”). An ANOVA yields a significant difference for the genotype for Iba1+CD68+ (F=14.1, 1 d.f., $p<0.01$), Iba1+CD68- (F=8, 1 d.f., $p<0.05$) and Iba1-CD68+ (F=6.65, 1 d.f., $p<0.05$). FAD patients exhibit an increase in Iba1+CD68+ surface and Iba1+CD68-surface in the high myelinated OT, and an increase in Iba1-CD68+ surface low myelinated OT, compared to Ctrl. (E) Quantification of Aβ surface that is overlapping with Iba1+CD68+ cells. An ANOVA yields a significant difference for the genotype for Aβ surface that is overlapping with Iba1+CD68+ cells (F=24.14, 1 d.f., $p<0.001$), Iba1+CD68- cells (F=9.93, 1 d.f., $p<0.01$) and Iba1-CD68+ cells (F=12.28, 1 d.f., $p<0.01$). An ANOVA yields a significant difference between high and low myelination areas for Aβ surface that is overlapping with Iba1+CD68- cells (F=8, 1 d.f., $p<0.05$) and Aβ free from microglial coverage (F=15.93, 1 d.f., $p<0.001$). Aβ surface that is overlapping with all three microglial populations is increased in the high myelin OT of FAD patients compared to Ctrl. Aβ surface that is overlapping with Iba1-CD68+ cells is increased in the low myelin OT. Aβ free from microglial coverage (arrows “4”) is decreased in the low myelin OT compared to the high myelin OT in both Ctrl and FAD. Scale bar: 50 μm.

Author Manuscript Author Manuscript Author Manuscript Author Manuscript

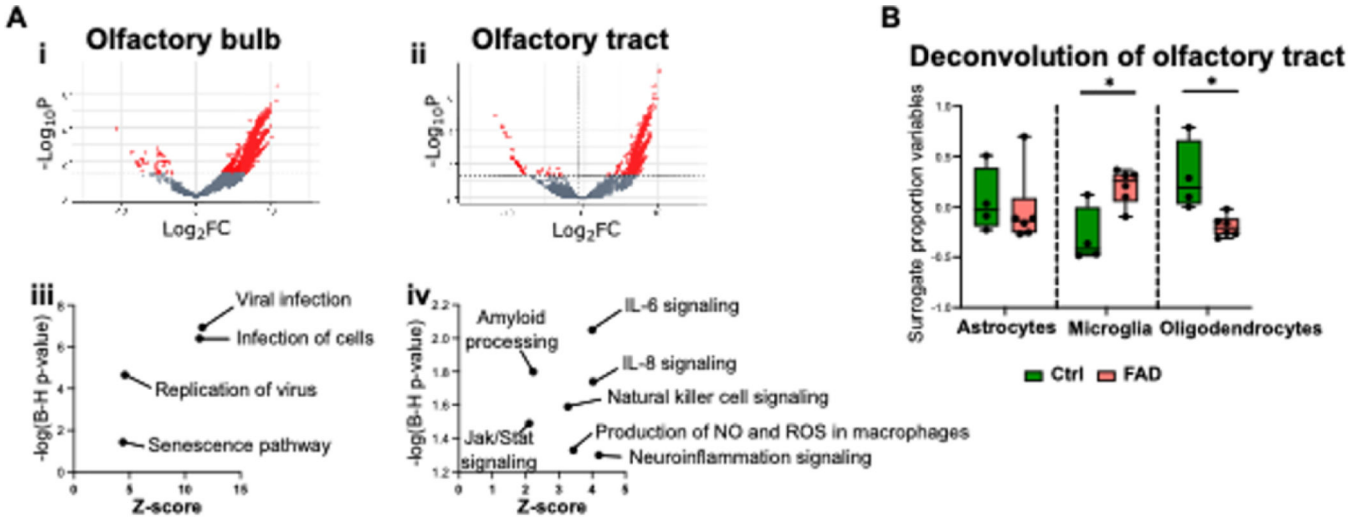

Figure 2.

Results of TempO-Seq transcriptomic analysis in the OB and OT of FAD patients and controls.

(A) Volcano plot for TempO-Seq (i, OB, ii, OT) and insight pathway analysis of transcriptional differences (iii, OB, iv, OT). (B) Deconvolution of the transcriptional differences for the OT. Asterisks are significant *p* values for post-hoc Fisher's least significant difference.

Author Manuscript
Author Manuscript
Author Manuscript
Author Manuscript

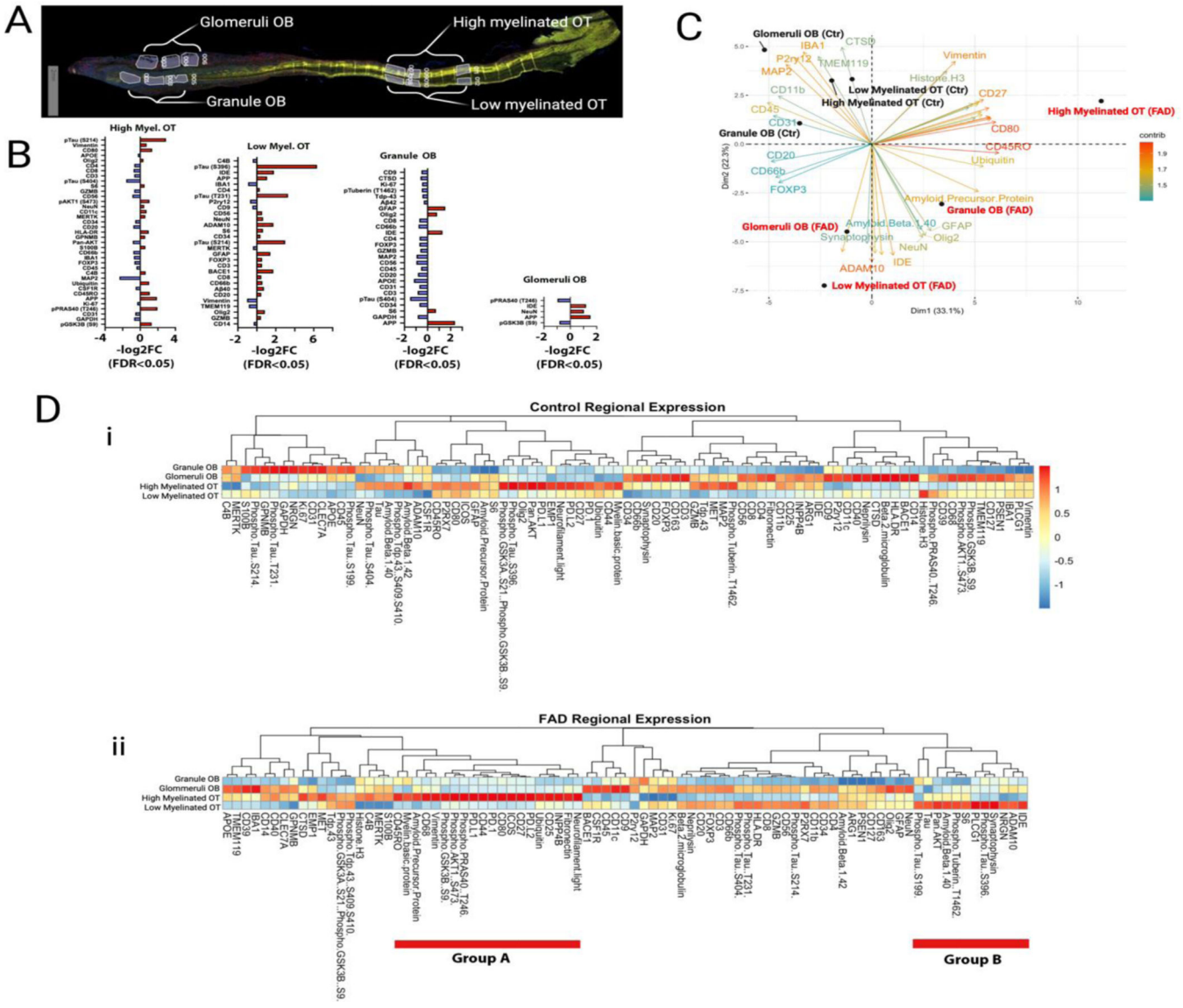

Figure 3.

nanoString Proteomic Analysis of OB and OT Expression of Markers for AD and Immunity

(A) Representative tissue section stained for myelin basic protein (MBP) showing the regions that were used for protein quantification. In the OB "Glomeruli OB" included the glomerular layer (GL) and the external plexiform layer (EPL), "Granule OB" included the granule cell layer and the accessory olfactory nucleus (AON). In the OT the high and low myelinated areas were determined by high and low MBP staining. (B) Log 2 fold change for the levels of protein expression in the different tissue regions. Red denotes higher expression in FAD. Only the proteins whose levels are significantly different between genotypes are shown. (C) Principal component analysis of the protein levels of expression. (D) Pseudocolor plots comparing between regions the levels of expression for all proteins. Proteins are segregated by Euclidean distance calculated by the total normalized reads for each protein between tissue regions or samples. i. Control tissue. ii. FAD. Group A are

Author Manuscript Author Manuscript Author Manuscript Author Manuscript

adjacent proteins that display higher levels in high myelinated OT and group B are adjacent proteins that display higher levels in low myelinated OT.

Author Manuscript Author Manuscript Author Manuscript Author Manuscript

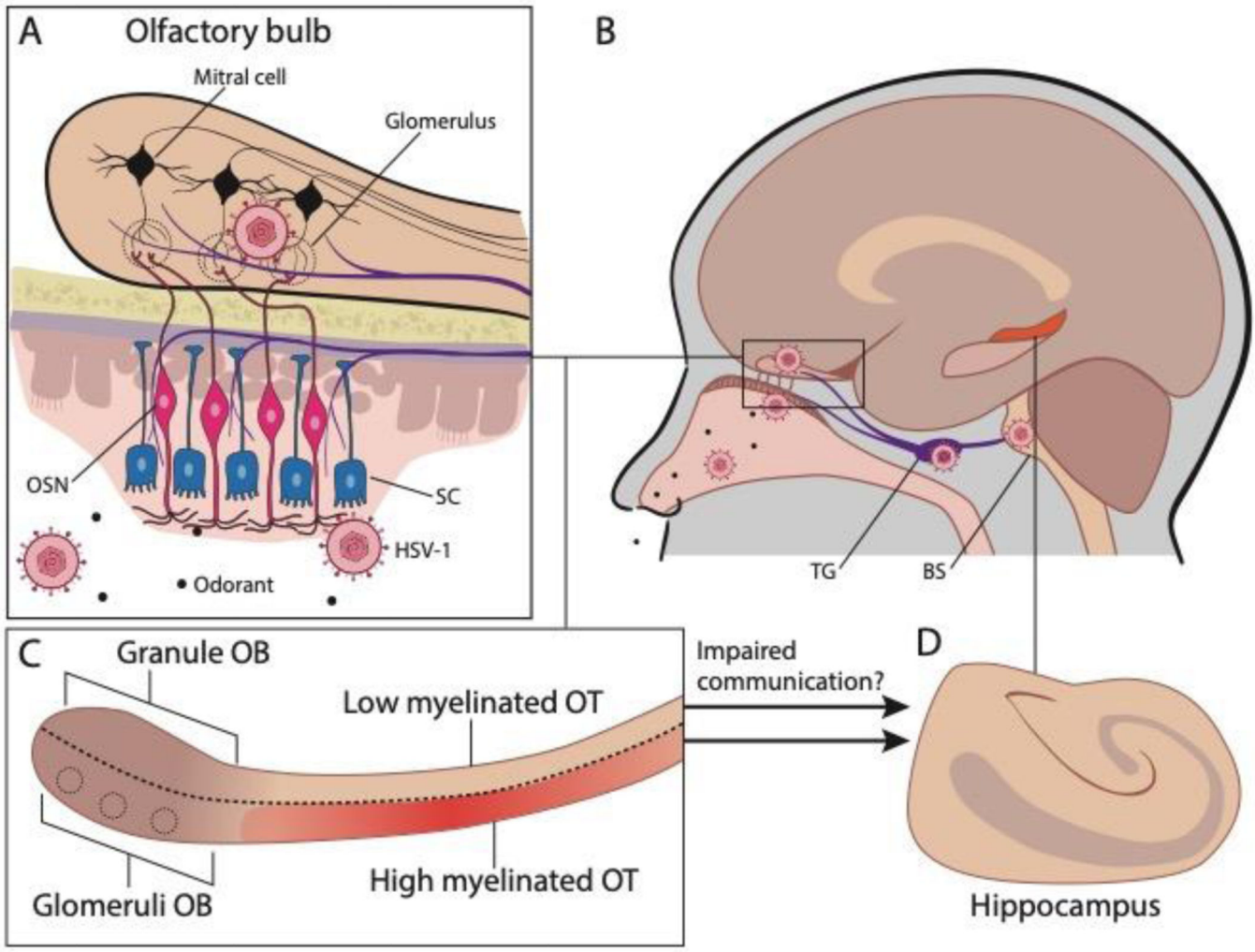

Figure 4.

Diagram illustrating the finding of a transcriptional signature of viral infection of the OB and inflammation and dysregulation of myelination in the OT of FAD patients. A. The olfactory epithelium bears direct neurotrophic entry of virus to the brain through either the axons of the olfactory sensory neurons that cross the cribriform plate and innervate the glomeruli in the OB, or through peripheral innervation from the trigeminal ganglion. OSN: olfactory sensory neuron. SC: sustentacular cell. B. Neurons in the trigeminal ganglion innervate the brainstem. TG: Trigeminal ganglion. BS: Brainstem. C. Mitral and tufted cells send information to downstream targets such as the piriform and entorhinal cortex through the olfactory tract. Entorhinal cortex innervates the hippocampus. We found that there was a transcriptional signature of viral infection in the OB of FAD patients (compared to controls). In addition, we found that in the aged individual the OT was partially myelinated, that in the FAD subjects there was an increase in transcripts involved in inflammation in the OT and that the response to demyelination in the OT differed between FAD subjects and controls. D. The findings raise the question whether the multisynaptic communication from

Author Manuscript Author Manuscript Author Manuscript Author Manuscript

the OT through the OT to the hippocampus is impaired in FAD patients and whether this impairment participates in cognitive disfunction.

Author Manuscript

Author Manuscript

Author Manuscript

Author Manuscript

Table 1

Patient Information

Subject ID	Group	Age	Sex	Cause of Death	OT surface analyzed in Vectra (mm2)	Temp-O-SEQ OT	Temp-O-SEQ OB	Nanostring OT	Nanostring OB
337	Control	84	M	Bacterial pneumonia	5.1	X	X	X	X
351	Control	62	M	Heart failure	7.0	X			
354	Control	65	M	Decompensated chronic obstructive pulmonary disease	3.3	X			
360	Control	72	M	Acute myocardial infarction	2.1		X		
364	Control	73	M	Gastric cancer	3.9		X		
380	Control	56	F	Colon cancer	4.1	X	X	X	X
359	FAD (E280A)	56	F	Bacterial pneumonia	3.6	X	X	X	X
346	FAD (E280A)	53	M	Aspiration pneumonia	5.2	X	X		
355	FAD (Late Onset)	86	F	Acute renal failure	3.0	X	X		
335	FAD (E280A)	59	M	Bacterial pneumonia	2.7	X	X		
358	FAD (E280A)	59	F	Aspiration pneumonia	1.1	X	X	X	X
382	FAD (E280A)	57	F	Metabolic imbalance	3.8	X	X		